A genetic screen suggests an alternative mechanism for inhibition of SecA by azide

Running title: Azide inhibits SecA by disrupting metal binding

Mohammed Jamshad[a], Rachael Chandler[a], Mark Jeeves[b], Ashley Robinson[a], Farhana Alam[a], Tamar Cranford Smith[a], Anokhi Shah[c], Oliver J. Daubney[d], Karl A. Dunne[a], Naomi Nabi[a*], Aadil Iqbal[a], Anna F. A. Peacock[d], Janet E. Lovett[c], Timothy Knowles[a], Ian Henderson[a] and Damon Huber[a#]

[a]Institute for Microbiology and Infection, [b]Institute of Cancer and Genomic Sciences and [d]School of Chemistry, University of Birmingham, Birmingham, United Kingdom; [c]SUPA, School of Physics and Astronomy, University of St Andrews, St. Andrews, United Kingdom

[#]Address correspondence to: Damon Huber, d.huber@bham.ac.uk

*Current address: Department of Biological Sciences, University of Huddersfield, Huddersfield, UK

Abstract

Sodium azide inhibits bacterial growth by inhibiting the activity of SecA, an ATPase required for translocation of proteins across the cytoplasmic membrane. To investigate the mechanism of action of azide, we used transposon directed insertion-site sequencing (TraDIS) to screen a high-density library of transposon insertion mutants for mutations that affect the susceptibility of *E. coli* to azide. Insertions in genes encoding most components of the Sec machinery increased susceptibility to azide. However, insertions truncating the C-terminal extension (CTE) of SecA decreased susceptibility of *E. coli* to azide. Insertions in genes encoding many metal binding proteins also increased susceptibility to azide, and transcriptional profiling suggested that treatment with azide disrupted iron homeostasis. The presence of iron in the media decreased the susceptibility of *E. coli* to azide, and mutations in the *secA* gene that confer resistance to azide altered the response of *E. coli* to iron limitation, suggesting a connection between iron metabolism and protein translocation. Although previous work suggests that SecA binds to zinc, SecA copurified with iron when expressed at physiological levels, and azide disrupted the interaction of the C-terminal metal-binding domain (MeBD) with iron *in vivo*. Biophysical analysis of metal binding by the MeBD using isothermal titration calorimetry and ^{1}H-nuclear magnetic resonance indicated a clear binding preference for Fe^{2+} over Zn^{2+}. These results indicate that the physiological ligand of SecA is iron and that azide inhibits SecA by disrupting iron binding.

Importance

Sodium azide is a common preservative that inhibits bacterial growth by inhibiting SecA, an ATPase that is required for transporting proteins across the cytoplasmic membrane. Previous

studies have suggested that azide inhibits the ATPase activity SecA by slowing the rate of nucleotide exchange. However, our results suggest that azide inhibits SecA by disrupting the structure of the C-terminal MeBD. It is thought that this domain binds to Zn^{2+}. However, our results indicate that the MeBD normally binds to Fe^{2+} and that azide disrupts the interaction of the MeBD with Fe^{2+}. Furthermore, mutations in the *secA* gene that confer azide resistance also cause a defect in the response of *E. coli* to iron depletion. SecA-dependent protein translocation is generally thought to be unregulated. However, these results suggest that the activity of SecA could be regulated in response to iron limitation.

Introduction

The Sec machinery is responsible for transporting proteins across (and inserting proteins into) the cytoplasmic membrane. In bacteria, the core Sec machinery consists of the integral membrane proteins SecY, SecE and SecG, which form a channel in the cytoplasmic membrane, and SecA, a soluble ATPase that either pushes (1) or to ratchets (2) proteins through the SecYEG channel (3-5). The structure of SecA can be divided into two regions. In *E.coli*, the catalytic core consists of the N-terminal ~830 amino acids. It contains the ATPase activity of the protein and is required for protein translocation (6-8). In addition, most SecAs contain a shorter C-terminal extension (CTE), which is not required for protein translocation (9). In *E. coli*, the CTE consists of a structurally flexible linker domain (FLD) of ~50 amino acids and a C-terminal metal-binding domain (MeBD) of ~20 amino acids (10), which coordinates a Zn^{2+} by a $CXCX_8CH$ motif (11). In *E. coli*, the CTE is required for the interaction of SecA with SecB (12), a chaperone that is required for the translocation of a subset of Sec substrates (13), and binding of the MeBD to Zn^{2+} stabilises this interaction (11). However, the MeBD is present in many species

that lack a SecB homologue (10, 14), suggesting that it has additional functions. Indeed, the near universal presence of the CTE (and the strong conservation of the variant found in *E. coli*) suggests a strong selective pressure for this function. It has been suggested that the CTE could inhibit the activity of the catalytic core (15). However, the physiological relevance of this autoinhibition and the conditions under which the CTE might autoinhibit SecA are unknown.

A number of "auxiliary" Sec components assist in protein translocation. Besides SecB, these include SecD, SecF, YidC and YajC, which form a supercomplex with SecYEG (16) and assist in the insertion of integral membrane proteins (16-20). In addition, the translocation of a subset of proteins, consisting mostly of integral membrane proteins, is dependent on a ribonucleoprotein complex known as the signal recognition particle (SRP) (21-23).

Sodium azide inhibits bacterial growth by inhibiting the activity of SecA (24, 25). Although azide interferes with a number of biological processes (26-33), mutations that confer azide resistance map almost exclusively to the *secA* gene (24, 25, 34), and azide causes a nearly complete block in SecA-mediated protein translocation within minutes of addition to growing cells (25). All of the mutations that have been identified to date alter amino acid residues located in the catalytic core of SecA, and most of these are located in one of its two nucleotide binding domains (24), which make up the ATPase. Azide inhibits F-ATPases and appears to do so by inhibiting nucleotide exchange (33). At very high concentrations (10-20 mM), azide also appears to inhibit nucleotide exchange by SecA *in vitro* (33, 35), and azide could act by a similar mechanism on SecA. However, the concentration of azide required to block SecA-dependent protein translocation *in vivo* (1-2 mM) is about an order of magnitude lower than the concentration required to partially inhibit SecA *in vitro* (25, 36), suggesting that azide has a different mechanism of action *in vivo*.

In this study, we screened a pool of ~1 million independent transposon-insertion mutants for mutations that increased sensitivity to azide using transposon-directed insertion site sequencing (TraDIS) (37). Insertions in genes encoding most components of the Sec machinery caused increased sensitivity to azide. However, insertions in the *secA* gene resulted in decreased sensitivity to azide. These insertions resulted in production of a protein lacking the CTE, suggesting a role for the CTE in sensitivity to azide. TraDIS also suggested that azide disrupts iron homeostasis, and transcriptional profiling indicated that this disruption occurs on the same time scale as inhibition of SecA. In addition, azide-resistant *secA* mutants display an altered response to iron limitation. These results led us to investigate the role of the MeBD in the inhibition of SecA by azide. We found that SecA preferentially binds to iron *in vitro* and *in vivo* and that treating cells with azide disrupts the interaction of the MeBD with iron *in vivo*. Taken together, our results suggest that azide inhibits SecA by sequestering iron from the C-terminal MeBD and disrupting its structure.

Results

Identification of genes that affect the susceptibility of *E. coli* to sodium azide using TraDIS. To identify insertion mutations that affected the susceptibility of *E. coli* to azide, we grew a library of >1 million independent transposon insertion mutants in the absence or presence of subinhibitory concentrations of azide. Mutants containing insertions that increase susceptibility to azide should grow more slowly in the presence of azide and therefore produce fewer progeny. Likewise, mutations that decrease susceptibility to azide should produce more progeny in the presence of azide. We therefore determined the number of progeny produced by each of the mutants in the library in a semi-quantitative fashion using Illumina sequencing.

Initial experiments indicated that concentrations of 1 mM sodium azide or greater almost completely inhibited the growth of *E. coli* in LB. However, 0.5 mM sodium azide caused partial growth inhibition; and concentrations of 0.25 mM or less had a minimal effect on growth (**supplemental figure S1A**). We therefore grew the TraDIS library in the presence of 0.25 mM or 0.5 mM sodium azide or in the absence of azide. A cursory examination of the data indicated that mutations affecting the Sec and cell envelope biogenesis machineries were depleted during growth in the presence azide (**supplemental figure S1B**), and a genome-wide comparison of the degree of depletion or enrichment (**figure 1A; supplemental data S1**) appeared to support this observation. Functional clustering analysis of the most depleted mutants using NCBI-DAVID (38) indicated that they affected genes in four functional categories: (i) protein translocation, (ii) cell envelope biogenesis, (iii) redox homeostasis and (iv) metal-ion binding proteins.

To confirm the results of our TraDIS screen, we examined the growth rates of a selected subset of single gene deletion mutants predicted by the TraDIS screen to have a growth defect in the presence of azide. Of the seven mutants tested (including those containing Δ*secG*, Δ*yajC*, Δ*dsbA*, Δ*cpxR*, Δ*gor*, Δ*ahpC* and Δ*trxC* mutations), six grew significant more slowly than the parent in the presence of azide (**supplemental table S1**). In addition, the growth defect of the Δ*yajC* mutant could be complemented by IPTG-inducible expression of *yajC* from a plasmid (**supplemental figure S1C**), indicating that the increased sensitivity of this mutant was not caused by polar effects on the expression of the downstream *secD* and *secF* genes (39). In contrast to the other *sec* mutants, cells containing insertions in the *secA* and *secB* genes became enriched during growth in azide (**figure 1A**). All of the insertions in *secA* that decreased susceptibility to azide were located in the region encoding the non-essential CTE, and the majority truncated the protein between amino acids 822 and 829 (**figure 1B**). Mutants containing

either (i) an IS*1* insertion in *secA* at codon 827 or (ii) a Δ*secB* deletion mutations grew significantly more rapidly than the parent in the presence of 0.5 mM azide (**figure 1C**). The close correlation between the sensitivity of the individual mutants to azide and the degree of depletion or enrichment in insertion mutants during growth in azide indicated that the results of the TraDIS screen were robust.

Transcriptional response of *E. coli* to azide. SecA is a metal binding protein, and oxidation of the metal-coordinating cysteines in the MeBD inactivates SecA *in vitro* (40). It was therefore possible that inhibition of SecA was the result of the effect of azide on metal-ion homeostasis or oxidative stress. However, because cells must be cultured in the presence of azide for TraDIS, it was also possible that either (or both) of these effects was indirect. In order to determine whether either effect occurred on the same time scale as inhibition of SecA, we investigated the transcriptional response of *E. coli* to azide using a DNA microarray (**supplemental data S2A**). Treatment of cells with 2 mM azide for 10 minutes resulted in a strong increase in the amount of the *secA* transcript. To determine the effect of azide on different regulatory networks (including responses to oxidative stress and disruptions in metal ion homeostasis), we identified the regulatory proteins controlling the expression of genes displaying the largest ($>\log_{10} 0.5$) change in mRNA levels (**supplemental data S2B**) and grouped the regulatory proteins into functional classes (**figure 2**; **supplemental data S2C**). The class of regulatory proteins that controlled the largest number of these genes (75) respond to changes in the respiratory state of the cell, and the class controlling the second-largest number of genes (57) were those that bind metal cofactors. These results indicated that the disruption of metal-ion homeostasis occurred on the same time scale as the disruption of SecA-dependent protein translocation. However, only ten genes were

controlled by proteins responding to oxidative stress, suggesting that the azide does not inhibit SecA by causing oxidative stress.

Effect of metal ion availability on sensitivity to azide. If azide inhibited SecA by perturbing metal-ion homeostasis, the availability of metal ions could affect the sensitivity of *E. coli* to azide. To investigate this possibility, we measured the zone of inhibition in a confluent lawn of cells surrounding a filter disc containing 10 μmol of sodium azide (**table 1**) (24). The presence of 1 mM EDTA in the plate caused a moderate but reproducible increase in the size of the zone of inhibition, consistent with the idea that azide affects metal-ion homeostasis. In addition, the presence of 100 μM $FeSO_4$ in the plate (but not $ZnSO_4$) caused a small but reproducible decrease in the sensitivity of *E. coli* to azide, suggesting that this effect was the result of a decrease in iron availability. We also examined the effect of EDTA on the growth of eight isogenic azide-resistant *secA* mutants (*azi-1*, *azi-4*, *azi-5*, *azi-7*, *azi-8*, *azi-16*, *azi-D1* and *azi-D2*). Two of these mutations were isolated for this study and contain C389T (*azi-D1*) and T556G (*azi-D2*) point mutations in the *secA* gene, which cause T130I and Y186D substitutions, respectively. The *azi-4* and *azi-5* alleles encode the same amino acid substitution at position 645 and served as internal controls. In contrast to the parent, the presence of EDTA decreased the sensitivity of most of the mutants to azide (**table 1**), suggesting that *azi* mutations alter the response of the mutants to metal limitation. This decreased sensitivity did not appear to be caused by a defect in Sec-dependent protein translocation since EDTA increased the sensitivity of other *sec* mutants to azide (**supplemental table S2**).

Effect of azide-resistant *secA* alleles on the response to iron limitation. To examine whether *azi* mutations alter the response of *E. coli* to iron limitation, we examined the growth of these mutants in M63 glucose minimal media from which we omitted iron (normally M63

contains ~3 μM $FeSO_4$ (41)). A Δ*entA* mutant, which cannot synthesise enterobactin, could not grow in this media in the absence of an alternative iron siderophore, such as citrate, indicating that growth in this media was dependent on enterobactin-dependent uptake of Fe^{3+}. The parent strain displayed three distinct exponential growth phases with two diauxic shifts in this media. The beginning of the first diauxic shift was marked by a decrease in growth rate at OD_{600} ~ 0.5 (**table 2**). The addition of 10 μM EDTA to the media decreased the growth rate during the first exponential growth phase but did not affect the cell density at which the first diauxic shift began (**figure 3A; table 2**), indicating that the rate of growth in the first growth phase was limited by metal-ion availability. However, the presence of 20 μM $FeCl_3$ in addition to 10 μM EDTA restored the growth rate in the first phase and caused the first diauxic shift to disappear (**figure 3A; table 2**). We obtained similar results when 10 μM $FeCl_3$ was added to the media in the absence of EDTA. Taken together, these results suggested that the first diauxic shift was the result of depletion of iron from the media and that the rate of growth in the first exponential phase was limited by the rate of iron uptake. The rates of growth of all of the *azi* mutants in the first growth phase, except *azi-7*, were indistinguishable from that of the parent both in the presence and absence of EDTA (**table 2**), indicating these mutations do not decrease the rate of iron uptake (e.g. by causing a defect in translocation). However, the length of the first diauxic shift for several *azi* mutants (*azi-1*, *azi-7*, *azi-8* and *azi-D1*) was significantly longer than that of the parent (see **figure 3B** for examples). Indeed, two of the mutants (*azi-1* and *azi-8*) did not recover at all during the course of the experiment. We obtained similar results using RPMI media, which is also iron-limited, and this effect could be enhanced by blocking enterobactin-dependent iron uptake in RPMI using mouse lipocalin-2 (42) (D. Huber, unpublished data).

SecA copurifies with iron. The MeBD of SecA is thought to bind Zn^{2+} (11, 40), but our results raised the possibility that the physiological ligand is iron. Iron-binding proteins are frequently mismetallated during purification because oxidation of the bound Fe^{2+} under aerobic conditions can reduce the affinity of the protein for the metal ion (43, 44). This reduction in affinity allows contaminating transition metals, which are more stable in aerobic conditions, to compete with iron for binding. In addition, SecA is normally produced at very high levels for purification, which could intensify the competition for free metal. In order to avoid these issues, we rapidly purify SecA from cells in which it was produced at more physiological levels. To this end, we used a variant of SecA that contains a biotin covalently attached at its C-terminus (SecA-biotin). SecA-biotin was produced from an IPTG-inducible copy of the *secA-biotin* gene, which was located on the chromosome. This gene was the sole copy of *secA* in this strain (45), and the strain required the presence of a minimum of 10 μM IPTG in the media for growth. In contrast to SecA produced from a plasmid (46), the addition of up to 1 mM IPTG did not have a detectable effect on growth. We rapidly purified SecA-biotin from cells grown in the presence of 10 μM and 1 mM IPTG using Streptactin-coupled sepharose beads. Streptactin is an engineered variant of streptavidin that has a similar affinity for biotin. After purification, the beads contained significant amounts of only two proteins: SecA-biotin and the biotin-carboxyl carrier protein (BCCP) (**supplemental figure S2**). Analysis of the zinc and iron content of the purified protein using optical emission spectroscopy (ICP-OES) indicated that iron was the major metal species present at both induction levels (**figure 4A**). Because BCCP is not known to bind to metal ions, the iron content of the sample was likely due to copurification with SecA.

Azide disrupts binding of the MeBD to iron *in vivo*. To investigate whether azide disrupts binding of the MeBD to iron, we determined the metal content of the CTE purified from cells

treated with 2 mM NaN_3 for 10 minutes. To aid in purification, the CTE was fused at its N-terminus to SUMO from *Saccharomyces cerevisiae*, which contained an N-terminal triple StrepTag II (Strep-SUMO-CTE). This fusion protein allowed relatively rapid purification of the CTE using Streptactin beads. We analysed the Mn, Fe, Ni, Co, Cu and Zn content of the eluted protein by mass spectrometry (ICP-MS). Only Zn^{2+} and Fe^{2+} were found in significant amounts. Furthermore, both ICP-MS and ICP-OES indicated a strong reduction in the amount of Fe copurified with the protein from azide-treated cells (**figure 4B**), suggesting that azide disrupts the interaction of SecA with iron *in vivo*. Furthermore, the Strep-SUMO-CTE purified from azide-treated cells was much more prone to aggregation than protein purified from untreated cells (**figure 4C**), suggesting that treatment with azide disrupts the structure of the CTE.

Effect of azide on the oxidation state of the MeBD. To investigate whether azide could directly oxidise the metal-coordinating cysteines in the MeBD, we measured the rate of metal release by purified Zn^{2+}-bound SecA. The presence of 20 mM azide did not detectably increase the basal rate of metal-ion release by SecA. Indeed, the rate of metal release in the presence of a strong oxidant (H_2O_2) was slow (apparent second order rate constant ~$0.024 \pm 0.006\ M^{-1}s^{-1}$) (**supplemental figure S3**), suggesting that the metal-coordinating cysteines are relatively refractory to oxidation. We could not detect any change in the oxidation state of the metal-coordinating cysteines of SecA from azide-treated cells *in vivo* (A. Iqbal and D. Huber, unpublished data).

Structural basis for the interaction of the MeBD with Fe^{2+}. We wished to investigate the metal-binding properties of the MeBD in more detail *in vitro*. To this end, we used a synthetic peptide consisting of the C-terminal 27 amino acids of SecA (MeBDwt; **figure 5A**). Isothermal titration calorimetry (ITC) indicated that the affinity of the MeBDwt peptide for Zn^{2+} was ~36

nM (**supplemental figure S4A**). We could not measure the interaction of MeBDwt with Fe^{2+} because oxidation of Fe^{2+} interfered with calorimetric measurements. However, the presence of 300 μM MeBDwt slowed the oxidation of 600 μM $FeSO_4$ under aerobic conditions, suggesting that MeBDwt could interact with Fe^{2+} (**supplemental figure S4B**). We could not detect any significant heat exchange apart from the heat of mixing when the MeBDwt peptide was mixed with $FeCl_3$, suggesting that MeBDwt has a much lower affinity for Fe^{3+} than for Zn^{2+}.

We next investigated the effect of Zn^{2+} and Fe^{2+} on the structure of the MeBDwt peptide using ^{1}H-NMR. The addition of Zn^{2+} to MeBDwt caused a significant change in the ^{1}H-NMR spectrum compared to the metal-free peptide, similar to what has been reported previously (10) (**supplemental figure S5A**). The addition of Fe^{2+} to the peptide resulted in a substantial quenching and broadening of ^{1}H signals, which was due to the paramagnetic properties of iron (**supplemental figure S5A**). A reduction in signal was not observed for a control peptide in the presence of Fe^{2+}, indicating this quenching and broadening for the MeBDwt peptide was due to interaction with Fe^{2+}. The presence of 10 mM NaN_3 also did not strongly affect the ^{1}H-NMR spectrum of the Zn^{2+}-bound peptide. However, it did cause some small perturbations in the ^{1}H-NMR spectrum Fe^{2+}-bound MeBDwt although the significance of these perturbations was unclear (**supplemental figure S5B**). The addition of 10 mM NaN_3 did not detectably affect the electron paramagnetic resonance (EPR) from the bound Fe^{2+} bound by the MeBDwt peptide (A. Shah, T. Cranford-Smith and J. E. Lovett, unpublished data), suggesting that azide does not directly oxidise the bound Fe^{2+}.

The signals from many of the ^{1}H atoms in the MeBDwt peptide could be assigned to particular amino acids. The hydrogens that showed the strongest loss of signal in the presence of Fe^{2+} were those in amino acids nearest to the Zn^{2+} ion in structural models of the MeBD (10, 47),

suggesting that the overall structure of the Fe^{2+}-bound is similar to that of the Zn^{2+}-bound peptide. The effect of the bound metal ion was particularly distinctive for the methyl hydrogens in valine, which were well separated in the ^{1}H-NMR spectrum (**figure 5B**). The addition of competing concentrations of Zn^{2+} to Fe^{2+}-bound MeBDwt peptide did not cause a detectable change in the ^{1}H-NMR spectrum, suggesting that the peptide preferentially binds to Fe^{2+} (**figure 5C**). B. R. Dempsey, et al. (10) previously noted the presence of a highly conserved serine residue at position 15 of the MeBDwt peptide (position 889 in full-length SecA; **figure 5A**). Because this residue is not directly involved in coordinating Zn^{2+} or in binding to SecB (47), we reasoned it could be important for determining the specificity of the MeBD for iron. An alanine substitution at this position (MeBD-S15A in **figure 5A**) allowed Zn^{2+} to more effectively compete with Fe^{2+} for binding to the peptide (**figure 5D**). In addition, the degree of quenching of the ^{1}H signals was less pronounced for the MeBD-S15A peptide compared to MeBDwt (compare the red lines in **figure 5C and 5D**), suggesting it has a lower affinity for Fe^{2+} than the wild-type peptide. However, the affinity of the MeBD-S15A peptide for Zn^{2+} ($K_D \sim 46$ nM) was nearly identical to that of the MeBDwt peptide in ITC experiments (**supplemental figure S4C**), suggesting that this serine is required for the specificity for Fe^{2+}.

Discussion

Our results suggest that the MeBD of SecA binds to iron and that azide inhibits the activity of SecA by disrupting the interaction of the MeBD with iron (**figure 6A**). When produced at physiological levels and purified rapidly to prevent air oxidation, SecA copurifies with iron, and biophysical analysis of the metal-binding properties of the MeBD suggested a marked binding preference for Fe^{2+} or over Zn^{2+}. TraDIS, transcriptional profiling and physiological experiments

all suggested that azide disrupts iron homeostasis, and iron availability affects the sensitivity of *E. coli* to azide. Finally, our TraDIS screen implicated the CTE of SecA in the sensitivity of *E. coli* to azide, and treating cells with azide disrupted the interaction of the MeBD with iron *in vivo*. Previous work suggested that the CTE inhibits the interaction of SecA with polypeptides *in vitro* and that the interaction of SecA with its binding partners, such as SecB, can relieve this inhibition (15). If this were the case, disrupting the structure of the MeBD would result in inhibition of SecA (e.g. because it could not interact effectively with its binding partners), but removal of the entire CTE would abrogate autoinhibition. In addition, mutations that destabilise the autoinhibited form of the protein would be expected to cause the protein to become less sensitive to sequestration of the bound iron (**figure 6B**). This model could explain why such a wealth of mutations that can confer azide resistance (e.g. see (24, 35, 48)). It is not clear why mutations that truncate SecA have not been isolated in previous screens for azide resistance, but it is possible that some degree of autoinhibition is required for survival in the presence of azide. Our results do not exclude the possibility that azide inhibits SecA by preventing nucleotide exchange, as has previously been suggested (24, 33, 35). However, they do raise the possibility that this mechanism may not be relevant *in vivo*.

Iron is an essential micronutrient, and iron availability is an important cue for changes in growth conditions (49-53). Our results suggest that autoinhibition of SecA could be involved in the physiological response of bacteria to changes in iron availability. All of the *azi* mutants that we tested altered the response of *E. coli* to metal limitation, and many *azi* mutants display defects in recovering from iron limitation. In addition, insertions truncating the *secA* gene were previously identified in a genetic screen for *Acinetobacter baumanii* mutants defective for growth under iron limitation (54). Finally, the SecA proteins of members of the

Lactobacillaceae, *Aerococcaceae* and *Leuconostocaceae* families of the lactic acid bacteria lack a CTE. These bacteria have a very low requirement for iron because they evolved to grow in milk, which is very limited for iron (55). Indeed, some *Lactobacillus* species appear to have lost the requirement for iron entirely (56). A relatively small number of species, including the Cyanobacteria, Chloroflexi, Chlamydiae and some branches of the high G/C Actinobacteria, contain SecAs with a different CTE. However, this does not rule out the possibility that these CTEs sense iron by a different mechanism.

Azide could disrupt binding of SecA to Fe^{2+} by at least two mechanisms. As noted by M. W. Bowler, et al. (33), azide inhibits many proteins due to its properties as a metal ligand (26-31). Although our results suggest that azide does not strongly affect the affinity of SecA for Fe^{2+}, it is possible that sequestration of iron by other iron-binding proteins results in indirect competition between these proteins and SecA *in vivo*. Alternatively, it is possible that oxidation of Fe^{2+} to Fe^{3+} in the presence of azide decreases the affinity of SecA for the bound iron. EPR experiments indicate that azide does not directly oxidise the bound Fe^{2+}. However, our TraDIS experiments suggest that treating cells with azide could result in the indirect oxidation of Fe^{2+}. Finally, it is possible that azide causes inhibition of SecA by a combination of these mechanisms *in vivo*.

Our finding that SecA binds to Fe^{2+} contradict previous work suggesting that Zn^{2+} is the physiological ligand of the MeBD (11). However, the protein used in this previous study was purified extensively under aerobic conditions (11). As a result, any iron initially present was likely oxidised Fe^{3+}, which has a lower affinity for the MeBD. In contrast to Fe^{2+}, Zn^{2+} is stable and soluble under aerobic conditions, and it is a common trace contaminant in buffers used for purification. In addition, many Fe^{2+}-binding proteins can also bind to Zn^{2+} (frequently with higher affinity) (57). Indeed, the apparent affinity of the MeBD for SecB in this study closely

mirrored the Irving-Williams series (Mn < Fe < Co < Ni < Cu = Zn) (11, 57, 58), suggesting that this assay measured the strength of the interaction between the peptide and the metal ion. Fe^{2+} and Zn^{2+} can occupy similar tetrahedral geometries (57), and our NMR experiments suggest that the structures of iron- and zinc-bound forms of the MeBD are likely very similar, which could explain why zinc-bound SecA is still functional *in vitro* (11, 47). Finally, the K_D of the complex between the MeBD and Zn^{2+} (nanomolar) is orders of magnitude higher than the intracellular concentration of Zn^{2+} predicted from the affinities of the Zn^{2+}-dependent regulators, such as Zur and ZntR (femtomolar) (57). However, the affinity of the MeBD for Fe^{2+} must be nanomolar or lower, which is consistent with the affinity of iron-dependent regulator proteins such as Fur (57, 58). Taken together, these results indicate that Fe^{2+}, and not Zn^{2+}, is the physiological ligand of SecA.

Methods

Chemicals and media. All chemicals were purchased from Fisher or Sigma-Aldrich unless indicated. Synthetic peptides were synthesised by Severn Biotech (Kidderminster, UK) or using an in house peptide synthesiser, and the quality of the peptides was checked in house using MALDI mass spectrometry. Cells were grown using LB or M63 media containing 0.2% glucose and 1 mg/ml arginine from which we omitted the addition of $FeSO_4$ (M63 (low iron)) (41, 59). Otherwise, where noted, NaN_3, isopropylthiogalactoside (IPTG), ethylenediaminetetraacetic acid (EDTA), $FeSO_4$, $FeCl_3$, $ZnSO_4$ or LCN-2 were added to the media at the indicated concentration. In general $FeSO_4$ was used instead of $FeCl_2$ because it was less prone to spontaneous oxidation. Where required, ampicillin (200 μg/ml) or kanamycin (30 μg/ml) were added to the growth media.

Strains and plasmids. Strains and plasmids were constructed using common methods (59, 60). Strain MG1115 (*secA827*::IS*1*) was a kind gift from M. Grabowicz and T. Silhavy (Princeton University). Single gene deletion mutants from the Keio collection (61) were obtained from the *E. coli* genetic stock centre (CGSC; Yale University, New Haven, Connecticut), as were strains AB251 (*azi-1*), AB4027 (*azi-5*), W208 SR Az^R (*azi-4*), JE1011 (*azi-16*), Hfr Hayes (*azi-7*) and χ2224 (*azi-8*). Novel azide-resistant *secA* mutants were selected as in J. L. Huie and T. J. Silhavy (24). The mutations in these *azi* mutants and the genotypes of DRH997 (*azi-D1*) and DRH998 (*azi-D2*) relative to the parent were confirmed using whole-genome sequencing (MicrobesNG, Birmingham). Plasmid pDH545 was constructed by PCR amplifying a fragment of the *secA* gene encoding the C-terminal 70 amino acids and cloning into plasmid pCA597 cut with *BsaI* and *BamHI* (62). A description of all the strains and plasmids used in this study can be found in **supplemental table S3** in the supplement.

TraDIS. TraDIS was carried out similar to G. C. Langridge, et al. (37). 50 ml of LB broth containing 0, 0.25 or 0.5 mM NaN_3 were inoculated with 10 μl of a library of ~1 million *E. coli* BW25113 mini-Tn*5* insertion mutants, and the cultures were grown to OD_{600} 1.0 or until growth ceased (OD_{600} ~ 0.9 for cultures grown in the presence of 0.5 mM NaN_3). Genomic DNA was extracted using a Qiagen QIAamp DNA blood mini kit and then processed using a two-step PCR method (63), which results in Illumina-compatible products. The PCR products were purified using the Agencourt AMPure XP system by Beckman Coulter and were sequenced using an Illumina MiSeq sequencer. Sequencing reads were mapped to the *E. coli* reference genome NC_007779.1 (*E. coli* K-12 substr. W3110). The number of insertions in the CDS for each gene was then determined. To reduce the amount of noise due to sequencing assignment errors, genes that exist in multiple copies on the chromosome (e.g. insertion elements and rRNA operons)

were eliminated from the analysis in **supplemental data S1.** In addition, genes containing 15 or fewer total insertions across all three conditions were eliminated in the data presented in **figure 1** and were not used for functional clustering analysis. BED files of the processed sequences aligned to NC_007779.1, the sequence file used for alignments and the features file used for assessing the location of the insertions are available at figshare.com (doi: 10.6084/m9.figshare.5280733).

Gene expression profiling. A 20 ml culture of *E. coli* BW25113 was grown to OD_{600} 0.8 and split into two 10 ml cultures. Half of the culture was incubated with 2 mM NaN_3 for 10 minutes after which the total RNA was prepped using a Qiagen RNEasy kit. Microarray analysis was carried out by the Functional Genomics and Proteomics Service (University of Birmingham, UK). cDNA was produced by arbitrary PCR using a poly-A primer from two technical RNA extraction replicates. cDNA from azide-treated cells was fluorescently labelled with Cy5, and cDNA from untreated cells was labelled with Cy3. It was then hybridised to an *E. coli* DNA microarray using a Two-Color Agilent Low Input Quick Amp Labeling Kit (Agilent), version 6. The slide was scanned using an Agilent Scanner C and Agilent Scan Control Software V.8.5 at a resolution of 3μm, and the data was extracted using Agilent Feature extraction software V 10.10. Expression data is available at NCBI-GEO.

Azide-sensitivity assay. The indicated strain was carefully swabbed on a plate from a fresh overnight culture using a disposable sterile cotton swab to produce an even lawn of bacteria. A 6 mm antibiotic assay (Merck-Millipore) was placed in the centre of the lawn, and 10 μl of a 1 M solution of NaN_3 was spotted on the filter disc. The diameter of the zone of clearing or of inhibition was determined by averaging the diameter measured at right angles. Azide resistance

assays were carried out using variants of *E. coli* MC4100 in order to keep the results as comparable as possible to J. L. Huie and T. J. Silhavy (24).

Growth in iron-limiting media. MC4100 or the indicated mutant were grown to saturation in M63 (low iron) containing 9 μM $FeCl_3$ and subcultured 1:100 into M63 (low iron) containing the indicated concentration of EDTA or $FeCl_3$. The cultures were grown shaking at 37˚C in 96-well round-bottom plates that were sealed a gas-permeable membrane in a BMG Labtech CLARIOStar plate reader, and the OD_{600} was measured every 10 minutes for 16 hours. Each measurement is the result of at least three independent cultures.

Determination of metal content of SecA-biotin and Strep-SUMO-CTE. To determine the metal content of full-length SecA-biotin, strain DRH839 was grown in the indicated concentration of IPTG to OD_{600} ~ 1 and lysed using cell disruption. Cell lysates were incubated with Streptactin-serpharose for 15 minutes on ice, and the sepharose beads were washed several times with buffer (50 mM HEPES, pH 7.5, 100 mM K·acetate, 10 mM Mg·acetate, 0.1% nonidet P40). Metal was eluted from the beads by incubating with metal elution buffer (10 mM HEPES, pH 7.5, 50 mM EDTA) at 55˚C for 30 minutes. Protein was eluted from the beads by boiling in SDS sample buffer, and the protein content was determined using a Bradford assay. To determine the effect of azide on binding of Strep-SUMO-CTE to iron, BL21(DE3) cells containing plasmid pDH543 was grown to OD_{600} 1.0, and production of Strep-SUMO-CTE was induced using 1 mM IPTG. After 1 hour, cultures were split, and half the culture was treated with 2 mM NaN_3 for 10 minutes. Cells were rapidly cooled, harvested by centrifugation and lysed using B-PER cell lysis reagent from Pierce (Rockford, Illinois). Cell lysates were incubated for 15 minutes with 50 μl of a 50% Streptactin-Sepharose slurry that had been pre-equilibrated with wash buffer (10 mM HEPES (potassium salt) pH 7.5, 100 mM potassium

acetate) and washed extensively with wash buffer or with wash buffer containing 10 mM NaN_3, as indicated. Next, the samples were washed using 10 mM HEPES (potassium salt) pH 7.5 and the excess liquid was dried using a SpeedVac. Total protein was eluted off of the column using using 10 mM HEPES (potassium salt) pH 7.5 buffer containing 7M guanidinium hydrochloride. The propensity to aggregate was determined by diluting 50 μl of the guanidinium-denatured protein into 950 μl of a 20 mM HEPES buffer and measuring light scattering at 500 nm. Where indicated, the metal content of the samples was determined using inductively coupled plasma-mass spectrometry (ICP-MS) or inductively coupled plasma-optical emission spectroscopy (ICP-OES) (School of Geography, Earth and Environmental Sciences, University of Birmingham, UK).

Zinc-release assay. Full-length SecA was purified similar to D. Huber, et al. (64) except that the protein was not subjected to an on-column denaturation step. SecA was charged with Zn^{2+} by incubating 40 μM of the purified protein with an equimolar concentration of $ZnCl_2$. Excess metal was removed from the protein using a 5 ml HiTrap Desalting Column (GE Healthcare). To measure the rate of Zn^{2+} release, 4 μM SecA was incubated in buffer containing 20 mM HEPES (potassium salt), pH 7.5, 100 mM potassium acetate, 20 mM magnesium acetate and 100 μM 4-(2-Pyridylazo)resorcinol (PAR) in the presence of the indicated concentration of H_2O_2 or in the presence of 20 mM NaN_3. The increase in PAR absorbance was measured every 60 s for 90 minutes at 492 nm using a BMG Labtech FLUOStar plate reader.

Isothermal titration calorimetry (ITC). ITC measurements were carried out in a MicroCal VP-ITC titration calorimeter (Piscataway, NJ, USA). All solutions were centrifuged for 5 min at 13,000 rpm and then thoroughly degassed under vacuum for 5 min with gentle stirring immediately before use. A solution of the indicated metal ion (0.1 mM) in the titration syringe

was titrated into a solution of the indicated peptide (0.01 mM) in the sample cell (Vo = 1.4037 ml). Both peptide and metal ion were dissolved in the same buffer (20 mM Na·HEPES, pH 7, 50 mM NaCl, 1.0 mM TCEP). Titrations consisted of a preliminary 2 µl injection followed by 50 6 µl injections of 12 s duration with 700 s between each injection. All experiments were carried out at 25˚C and an initial reference power of 10 µcal/sec. The raw data was analysed with Origin 7.0 using one-binding site model and was corrected for the heat of dilution of the metal ion in the absence of peptide.

^{1}H-NMR. All NMR spectra were carried out on a Bruker 900 MHz spectrometer at 25 °C using a cryogenically cooled 5mm TCI probe and excitation sculpting for water suppression on a sample in 90% H_2O/10% D_2O. Sequence specific assignments were completed using a TOCSY experiment in 90% H_2O/10% D_2O using a DIPSI2 spin-lock with a mixing time of 65 ms. The data set was comprised of 32 transients and 512 increments with a spectral width of 10 ppm. 1D data sets comprised 16 transients, 32k data points and a spectral width of 16 ppm. All 1D data were processed using Topspin 3.2.6 software using an exponential window function with a line broadening of 1 Hz.

Western blotting. Samples were resolved by SDS-PAGE and blotted to nitrocellulose. Membranes were then developed using a primary α-SecA (rabbit) antiserum and a secondary horseradish peroxidase coupled anti-rabbit antiserum (GE Healthcare) (60).

Funding information

This work was funded by the BBSRC (grant BB/L019434/1 to D. Huber, M. Jamshad and R. Chandler and an MIBTP studentship to T. Cranford Smith), the EPSRC (DTP EP/M508214/1 to A. Shah), the Royal Society (University Research Fellowship to J. E. Lovett), the DSTL (to O.

B. Daubney) and the Wellcome Trust (grant 099149/Z/12/Z for the Q-band EPR spectrometer and grant 099185/Z/12/Z for the 900 MHz NMR spectrometer). The funders had no role in study design, data collection and interpretation, or the decision to submit the work for publication.

Acknowledgements

We thank Dr. S. Baker, Dr. M. Thompson and Dr. H. El Mkami for technical assistance. We also thank Prof. D. Collison and members of the Henderson and Lund labs for helpful discussions. We thank HWB-NMR at the University of Birmingham for providing open access to their Wellcome Trust-funded 900 MHz spectrometer.

References

1. **Bauer BW, Shemesh T, Chen Y, Rapoport TA.** 2014. A "push and slide" mechanism allows sequence-insensitive translocation of secretory proteins by the SecA ATPase. Cell **157:**1416-1429.
2. **Allen WJ, Corey RA, Oatley P, Sessions RB, Baldwin SA, Radford SE, Tuma R, Collinson I.** 2016. Two-way communication between SecY and SecA suggests a Brownian ratchet mechanism for protein translocation. Elife **5**.
3. **Collinson I, Corey RA, Allen WJ.** 2015. Channel crossing: how are proteins shipped across the bacterial plasma membrane? Philos Trans R Soc Lond B Biol Sci **370**.
4. **Beckwith J.** 2013. The Sec-dependent pathway. Res Microbiol **164:**497-504.
5. **Van den Berg B, Clemons WM, Jr., Collinson I, Modis Y, Hartmann E, Harrison SC, Rapoport TA.** 2004. X-ray structure of a protein-conducting channel. Nature **427:**36-44.

6. **Grabowicz M, Yeh J, Silhavy TJ.** 2013. Dominant negative lptE mutation that supports a role for LptE as a plug in the LptD barrel. J Bacteriol **195:**1327-1334.

7. **Or E, Boyd D, Gon S, Beckwith J, Rapoport T.** 2005. The bacterial ATPase SecA functions as a monomer in protein translocation. J Biol Chem **280:**9097-9105.

8. **Or E, Navon A, Rapoport T.** 2002. Dissociation of the dimeric SecA ATPase during protein translocation across the bacterial membrane. Embo J **21:**4470-4479.

9. **Hirano M, Matsuyama S, Tokuda H.** 1996. The carboxyl-terminal region is essential for Sec-A dimerization. Biochem Biophys Res Commun **229:**90-95.

10. **Dempsey BR, Wrona M, Moulin JM, Gloor GB, Jalilehvand F, Lajoie G, Shaw GS, Shilton BH.** 2004. Solution NMR structure and X-ray absorption analysis of the C-terminal zinc-binding domain of the SecA ATPase. Biochemistry **43:**9361-9371.

11. **Fekkes P, de Wit JG, Boorsma A, Friesen RH, Driessen AJ.** 1999. Zinc stabilizes the SecB binding site of SecA. Biochemistry **38:**5111-5116.

12. **Fekkes P, van der Does C, Driessen AJ.** 1997. The molecular chaperone SecB is released from the carboxy-terminus of SecA during initiation of precursor protein translocation. Embo J **16:**6105-6113.

13. **Randall LL, Hardy SJ.** 2002. SecB, one small chaperone in the complex milieu of the cell. Cell Mol Life Sci **59:**1617-1623.

14. **van der Sluis EO, Driessen AJ.** 2006. Stepwise evolution of the Sec machinery in Proteobacteria. Trends Microbiol **14:**105-108.

15. **Gelis I, Bonvin AM, Keramisanou D, Koukaki M, Gouridis G, Karamanou S, Economou A, Kalodimos CG.** 2007. Structural basis for signal-sequence recognition by the translocase motor SecA as determined by NMR. Cell **131:**756-769.

16. **Komar J, Alvira S, Schulze RJ, Martin R, Lycklama ANJA, Lee SC, Dafforn TR, Deckers-Hebestreit G, Berger I, Schaffitzel C, Collinson I.** 2016. Membrane protein insertion and assembly by the bacterial holo-translocon SecYEG-SecDF-YajC-YidC. Biochem J **473:**3341-3354.

17. **Hennon SW, Soman R, Zhu L, Dalbey RE.** 2015. YidC/Alb3/Oxa1 Family of Insertases. J Biol Chem **290:**14866-14874.

18. **Tsukazaki T, Mori H, Echizen Y, Ishitani R, Fukai S, Tanaka T, Perederina A, Vassylyev DG, Kohno T, Maturana AD, Ito K, Nureki O.** 2011. Structure and function of a membrane component SecDF that enhances protein export. Nature **474:**235-238.

19. **Schulze RJ, Komar J, Botte M, Allen WJ, Whitehouse S, Gold VA, Lycklama ANJA, Huard K, Berger I, Schaffitzel C, Collinson I.** 2014. Membrane protein insertion and proton-motive-force-dependent secretion through the bacterial holo-translocon SecYEG-SecDF-YajC-YidC. Proc Natl Acad Sci U S A **111:**4844-4849.

20. **Duong F, Wickner W.** 1997. Distinct catalytic roles of the SecYE, SecG and SecDFyajC subunits of preprotein translocase holoenzyme. Embo J **16:**2756-2768.

21. **Huber D, Boyd D, Xia Y, Olma MH, Gerstein M, Beckwith J.** 2005. Use of thioredoxin as a reporter to identify a subset of Escherichia coli signal sequences that promote signal recognition particle-dependent translocation. J Bacteriol **187:**2983-2991.

22. **Ulbrandt ND, Newitt JA, Bernstein HD.** 1997. The E. coli signal recognition particle is required for the insertion of a subset of inner membrane proteins. Cell **88:**187-196.

23. **Saraogi I, Shan SO.** 2014. Co-translational protein targeting to the bacterial membrane. Biochim Biophys Acta **1843:**1433-1441.

24. **Huie JL, Silhavy TJ.** 1995. Suppression of signal sequence defects and azide resistance in Escherichia coli commonly result from the same mutations in secA. J Bacteriol **177:**3518-3526.

25. **Oliver DB, Cabelli RJ, Dolan KM, Jarosik GP.** 1990. Azide-resistant mutants of Escherichia coli alter the SecA protein, an azide-sensitive component of the protein export machinery. Proc Natl Acad Sci U S A **87:**8227-8231.

26. **Yoshikawa S, Caughey WS.** 1992. Infrared evidence of azide binding to iron, copper, and non-metal sites in heart cytochrome c oxidase. J Biol Chem **267:**9757-9766.

27. **Stannard JN, Horecker BL.** 1948. The in vitro inhibition of cytochrome oxidase by azide and cyanide. J Biol Chem **172:**599-608.

28. **Michaelis EK.** 1979. The glutamate receptor-like protein of brain synaptic membranes is a metalloprotein. Biochem Biophys Res Commun **87:**106-113.

29. **Wever R, Muijsers AO, van Gelder BF, Bakker EP, van Buuren KJ.** 1973. Biochemical and biophysical studies on cytochrome c oxidase. XI. Reaction with azide. Biochim Biophys Acta **325:**1-7.

30. **Little RH, Cheesman MR, Thomson AJ, Greenwood C, Watmough NJ.** 1996. Cytochrome bo from Escherichia coli: binding of azide to CuB. Biochemistry **35:**13780-13787.

31. **Nicholls P.** 1964. The reaction of azide with catalase and their significance. Biochem J **90:**331-343.

32. **Reid RJ, Loughman BC, Ratcliffe RG.** 1985. 31P NMR Measurements of Cytoplasmic pH Changes in Maize Root Tips. J Exp Botany **36:**889-897.

33. **Bowler MW, Montgomery MG, Leslie AG, Walker JE.** 2006. How azide inhibits ATP hydrolysis by the F-ATPases. Proc Natl Acad Sci U S A **103:**8646-8649.

34. **Fortin Y, Phoenix P, Drapeau GR.** 1990. Mutations conferring resistance to azide in Escherichia coli occur primarily in the secA gene. J Bacteriol **172:**6607-6610.

35. **Schmidt M, Ding H, Ramamurthy V, Mukerji I, Oliver D.** 2000. Nucleotide binding activity of SecA homodimer is conformationally regulated by temperature and altered by prlD and azi mutations. J Biol Chem **275:**15440-15448.

36. **van der Wolk JP, de Wit JG, Driessen AJ.** 1997. The catalytic cycle of the escherichia coli SecA ATPase comprises two distinct preprotein translocation events. EMBO J **16:**7297-7304.

37. **Langridge GC, Phan MD, Turner DJ, Perkins TT, Parts L, Haase J, Charles I, Maskell DJ, Peters SE, Dougan G, Wain J, Parkhill J, Turner AK.** 2009. Simultaneous assay of every Salmonella Typhi gene using one million transposon mutants. Genome Res **19:**2308-2316.

38. **Huang da W, Sherman BT, Lempicki RA.** 2009. Bioinformatics enrichment tools: paths toward the comprehensive functional analysis of large gene lists. Nucleic Acids Res **37:**1-13.

39. **Pogliano KJ, Beckwith J.** 1994. Genetic and molecular characterization of the Escherichia coli secD operon and its products. J Bacteriol **176:**804-814.

40. **Woodbury RL, Hardy SJ, Randall LL.** 2002. Complex behavior in solution of homodimeric SecA. Protein Sci **11:**875-882.

41. **Pardee AB, Jacob F, Monod J.** 1959. Genetic Control and Cytoplasmic Expression of Inducibility in the Synthesis of Beta-Galactosidase by E-Coli. Journal of Molecular Biology **1:**165-178.

42. **Flo TH, Smith KD, Sato S, Rodriguez DJ, Holmes MA, Strong RK, Akira S, Aderem A.** 2004. Lipocalin 2 mediates an innate immune response to bacterial infection by sequestrating iron. Nature **432:**917-921.

43. **Imlay JA.** 2014. The mismetallation of enzymes during oxidative stress. J Biol Chem **289:**28121-28128.

44. **Gu M, Imlay JA.** 2013. Superoxide poisons mononuclear iron enzymes by causing mismetallation. Mol Microbiol **89:**123-134.

45. **Huber D, Jamshad M, Hanmer R, Schibich D, Doring K, Marcomini I, Kramer G, Bukau B.** 2017. SecA Cotranslationally Interacts with Nascent Substrate Proteins In Vivo. J Bacteriol **199**.

46. **Gouridis G, Karamanou S, Sardis MF, Scharer MA, Capitani G, Economou A.** 2013. Quaternary dynamics of the SecA motor drive translocase catalysis. Mol Cell **52:**655-666.

47. **Zhou J, Xu Z.** 2003. Structural determinants of SecB recognition by SecA in bacterial protein translocation. Nat Struct Biol **10:**942-947.

48. **Das S, Grady LM, Michtavy J, Zhou Y, Cohan FM, Hingorani MM, Oliver DB.** 2012. The variable subdomain of Escherichia coli SecA functions to regulate SecA ATPase activity and ADP release. J Bacteriol **194:**2205-2213.

49. **Kustka A, Carpenter EJ, Sanudo-Wilhelmy SA.** 2002. Iron and marine nitrogen fixation: progress and future directions. Res Microbiol **153:**255-262.

50. **Briat JF, Ravet K, Arnaud N, Duc C, Boucherez J, Touraine B, Cellier F, Gaymard F.** 2010. New insights into ferritin synthesis and function highlight a link between iron homeostasis and oxidative stress in plants. Ann Bot **105:**811-822.

51. **Moisescu C, Ardelean, II, Benning LG.** 2014. The effect and role of environmental conditions on magnetosome synthesis. Front Microbiol **5:**49.

52. **Kortman GA, Raffatellu M, Swinkels DW, Tjalsma H.** 2014. Nutritional iron turned inside out: intestinal stress from a gut microbial perspective. FEMS Microbiol Rev **38:**1202-1234.

53. **Raffatellu M, George MD, Akiyama Y, Hornsby MJ, Nuccio SP, Paixao TA, Butler BP, Chu H, Santos RL, Berger T, Mak TW, Tsolis RM, Bevins CL, Solnick JV, Dandekar S, Baumler AJ.** 2009. Lipocalin-2 resistance confers an advantage to Salmonella enterica serotype Typhimurium for growth and survival in the inflamed intestine. Cell Host Microbe **5:**476-486.

54. **Fiester SE, Nwugo CC, Penwell WF, Neary JM, Beckett AC, Arivett BA, Schmidt RE, Geiger SC, Connerly PL, Menke SM, Tomaras AP, Actis LA.** 2015. Role of the carboxy terminus of SecA in iron acquisition, protein translocation, and virulence of the bacterial pathogen Acinetobacter baumannii. Infect Immun **83:**1354-1365.

55. **Lisher JP, Giedroc DP.** 2013. Manganese acquisition and homeostasis at the host-pathogen interface. Frontiers in Cellular and Infection Microbiology **3**.

56. **Weinberg ED.** 1997. The Lactobacillus anomaly; Total iron abstinence. Perspectives in Biology and Medicine **40:**578-583.

57. **Waldron KJ, Rutherford JC, Ford D, Robinson NJ.** 2009. Metalloproteins and metal sensing. Nature **460:**823-830.

58. **Waldron KJ, Robinson NJ.** 2009. How do bacterial cells ensure that metalloproteins get the correct metal? Nat Rev Microbiol **7:**25-35.

59. **Miller JH.** 1992. A Short Course in Bacterial Genetics. Cold Spring Harbor Press, Cold Spring Harbor, NY.

60. **Sambrook J, Russell DW.** 2001. Molecular Cloning: A Laboratory Manual, 3rd ed. Cold Spring Harbor Press, Cold Spring Harbor, NY.

61. **Baba T, Ara T, Hasegawa M, Takai Y, Okumura Y, Baba M, Datsenko KA, Tomita M, Wanner BL, Mori H.** 2006. Construction of Escherichia coli K-12 in-frame, single-gene knockout mutants: the Keio collection. Mol Syst Biol **2:**2006 0008.

62. **Andreasson C, Fiaux J, Rampelt H, Mayer MP, Bukau B.** 2008. Hsp110 is a nucleotide-activated exchange factor for Hsp70. J Biol Chem **283:**8877-8884.

63. **Christen B, Abeliuk E, Collier JM, Kalogeraki VS, Passarelli B, Coller JA, Fero MJ, McAdams HH, Shapiro L.** 2011. The essential genome of a bacterium. Mol Syst Biol **7:**528.

64. **Huber D, Rajagopalan N, Preissler S, Rocco MA, Merz F, Kramer G, Bukau B.** 2011. SecA interacts with ribosomes in order to facilitate posttranslational translocation in bacteria. Mol Cell **41:**343-353.

Figure legends

Figure 1. Effect of insertion mutations on growth in the presence of azide. (A & B) A library of >1 million independent mini-Tn*5* insertion mutants was grown in the absence or presence of 0.25 or 0.5 mM NaN_3, and the number of cells containing insertions at each site in the final culture was counted using Illumina sequencing. (A) The change in the number of insertions in each gene was quantified by taking of the fraction of the number of insertions in a gene after growth in the presence of 0.5 mM azide over the number of insertions in the gene after growth in the absence of azide. The $\log_2$ of this fraction was plotted in order of increasing enrichment. The location of several representative genes (*secA*, *secB*, *secF*, *secG*, *secM*, *yidC*, *yajC*, *cpxR*, *dsbA*, *ahpC*, *gor* and *trxC*) are indicated. (B) Profile of mini-Tn*5* insertions in the *secA* gene after growth of the TraDIS library in the absence (black) or presence of 0.25 (blue) or 0.5 mM (red) NaN_3. The approximate location of codon 822 is indicated. (C) Doubling times of MC4100 (parent), DRH1075 (MC4100 *secA827*::IS*1*) and DRH918 (MC4100 Δ*secB*::Kan^R) in LB in the presence of 0.5 mM NaN_3. The approximate doubling time of all three strains in the absence of azide is indicated by the dotted line. Error bars are one s.d.

Figure 2. Graphical representation of the classes of regulatory proteins controlling the genes displaying the largest change in expression after treatment with azide. A culture of cells growing was grown to exponential phase in LB. Half of the culture was left untreated and the other half was treated with 2 mM NaN_3 for 10 minutes. The mRNA profiles of the two samples were then determined using a DNA microarray. The regulatory proteins controlling the expression of genes displaying a > ~3-fold ($\log_{10}$ 0.5) increase or decrease change in mRNA levels were determined and sorted into the indicated functional classes. For each functional class,

each colour represents a different regulator protein. Full details of the analysis can be found in **supplemental data S2.**

Figure 3. Example growth curves of *E. coli* MC4100 and *azi* mutants in M63 (low Fe). Cells were grown in M63 minimal salts lacking $FeSO_4$ and containing 0.2% glucose (M63-Fe) at 37˚C in a 96-well microtiter dish, and growth was determined by measuring the OD_{600}. The log_2 of the OD_{600} is plotted versus time. (A) Growth of the parent strain (MC4100) in M63-Fe (solid black line) or M63-Fe to which 10 μM EDTA (dotted grey line) or 10 μM EDTA and 20 μM $FeCl_3$ (grey line) were added. The approximate locations of the two diauxic shifts in M63-Fe are indicated with arrows. (B) Growth of the MC4100 (parent; solid black line), DRH1019 (*azi-7*; dotted grey line) and DRH1020 (*azi-8*; solid grey line) in M63-Fe. Parameters determined from these growth curves are given in **Table 2**.

Figure 4. Interaction of SecA with iron *in vivo*. (A) DRH839 (p_{lac}-*secA-biotin*) was grown to OD_{600} ~ 1 in the presence of either 10 μM or 1 mM IPTG, as indicated. SecA-biotin was rapidly purified from the cell lysates using Streptactin-sepharose media. The iron and zinc content of the samples was determined using optical emission spectroscopy (ICP-OES) and was normalised to the total protein content. (B & C) Cells producing Strep-SUMO-CTE were incubated in the absence (untreated) or presence of 2 mM NaN_3 for 10 minutes. Strep-SUMO-CTE was purified from the cell lysates using Streptactin resin and washed extensively with buffer. (B) The iron content of the samples was determined using mass spectrometry (ICP-MS) and normalised to the protein content of the sample as determined by Bradford assay. Confidence intervals are one s.d. (C) The bound protein was eluted from the resin by denaturation using 7M guanidinium and then

diluted to renaturing conditions. Aggregation of the protein was determined by measuring light scattering at 500 nm. Confidence intervals are the s.e.m.

Figure 5. NMR analysis of Fe^{2+}-binding activity of the MeBD of SecA (A) Clustal omega alignment of the MeBDs from *E. coli*, *Rhizobium loti*, *Bacillus subtilis*, *Lactococcus lactis*, *Treponema pallidum*, *Bifidobacterium longum* and *Bacteroides thetaiotamicron* . The sequence of the S15A peptide is shown in alignment below. Positions of the known metal-coordinating residues are bolded. The conserved serine (position 889 in full length SecA) is depicted in red. (B, C &D) ^{1}H-NMR spectra of the region corresponding to the valine hydrogens. (B) ^{1}H-NMR spectra of 1 mM MeBDwt peptide in the absence of metal (blue) or presence of 1.2 mM $FeSO_4$ (red) or $ZnSO_4$ (green). (C & D) ^{1}H-NMR spectra of 1 mM MeBDwt (C) or MeBD-S15A (D) in the absence of metal (Apo, blue) or in the presence of 1.2 mM $FeSO_4$ (red). Alternatively, 1.2 mM competing $ZnSO_4$ was added to peptide that had been preincubated with 1.2 mM $FeSO_4$ (purple). Chemical shifts (ppm) are aligned to panel D and indicated below.

Figure 6. Diagram of the proposed mechanism of action of azide. See text for full description. (A) Full-length SecA exists in two states: an inactive “apo” state and an active Fe^{2+}-bound state. Under normal growth conditions, SecA occupies the active state. However, treatment of cells with azide results in sequestration of iron from SecA and inactivation of the protein. Not depicted: removal of the CTE results in a protein that is constitutively active. (B) Single amino acid substitutions and small deletions destabilise the inactive form of SecA and cause it to be partially active even in the “apo” state.

Legends for supplemental items

Figure S1. Effect of sodium azide concentration on growth. (A) Strain BW25113 was cultured in LB in the absence (red) or presence of 0.0625 mM (orange), 0.125 mM (yellow), 0.25 (green), 0.5 (cyan), 1.0 (blue) or 10 mM (purple) sodium azide. The optical density at 600 nm (OD_{600}) was measured approximately every 30 minutes. (B) Number of insertions at each location in the *secG*, *yajC* and *cpxR* genes after growth of the TraDIS library in the absence (black) or presence of 0.25 (blue) or 0.5 (red) mM NaN_3. The scale of the x-axis differs in each example. (C) Complementation of the azide-dependent growth defect of a Δ*yajC* mutant. The parent (BW25113; WT) and Δ*yajC* mutant strains were transformed with either a plasmid conferring IPTG-inducible expression of the *yajC* gene (pTrc-YajC) or the empty vector (pTrc99a), as indicated, and grown in the presence of 0.25 mM NaN_3. Expression of the *yajC* gene was induced using 0.05, 0.1, 0.2 or 1 mM IPTG, as indicated.

Figure S2. Defects oxidative stress response machinery cause increase sensitivity to azide. Strain DRH839 was grown to OD_{600} = 1 in LB in the presence of 10 μM or 1 mM IPTG, as indicated. SecA-biotin was purified from the cell lysates using streptactin-sepharose beads. The purified protein was resolved using SDS-PAGE and stained using a Coomassie stain. Dilutions of each sample corresponding to the indicated amount of protein were loaded on the gel to detect the presence of less prominent bands. The running positions of SecA-biotin and the biotin-carboxyl carrier protein (BCCP) are indicated.

Figure S3. Rate of Zn^{2+} release by SecA during incubation in the presence of different concentrations of hydrogen peroxide. 4 μM SecA that was pre-charged with Zn^{2+} was

incubated in the absence or presence of 50 mM, 10 mM or 2 mM hydrogen peroxide or 20 mM NaN_3. The concentration of free Zn^{2+} released upon oxidation of the cysteines in the MeBD was determined by measuring the increase in PAR absorbance and 492 nm.

Supplemental figure S4. Binding of the MeBDwt and MeBD-S15A peptides to iron and zinc. (A & C) The affinity of MeBDwt (A) and MeBD-S15A (C) were determined using isothermal titration calorimetry by titrating a $ZnSO_4$ solution into metal-free peptide at a concentration of 10 μM. After subtracting the heat of injection of $ZnSO_4$ from the raw data, the binding parameters were calculated assuming that there is one metal binding site per peptide. The calculated K_D, ΔH and ΔS of the complexes are indicated. Confidence intervals are 1 s.d. (B) 600 μM $FeSO_4$ was incubated on its own in buffer or in the presence of 300 μM MeBDwt peptide for 30 minutes at room temperature under aerobic conditions. The yellow colour of the solution is an indication of the formation of Fe^{3+}.

Figure S5. ^{1}H-NMR suggests the MeBD binds to iron and that azide affect the structure of the iron-bound peptide. (A) ^{1}H-NMR spectra of the amide hydrogen region for the WT MeBD peptide. 1 mM peptide was incubated in the absence (blue) or presence of 1.2 mM $FeSO_4$ (red) or $ZnSO_4$ (green). (B) ^{1}H-NMR spectra of 1 mM WT MeBD peptide in the presence of 1.2 mM $FeSO_4$ in the absence (red) or presence (blue) of 20 mM NaN_3.

Table S1. Relative growth rates of single gene deletion mutants from the Keio collection.

Table S2. Effect of EDTA on the sensitivity of *E. coli* BW25113 and *sec* mutants.

Table S3. Strains and plasmids used in this study.

Data S1. Summary of TraDIS results. (A) Number of insertions per gene for two independent Illumina sequencing runs. The number of sequencing reads for all three conditions for each run was similar. However, to make the number of reads for each condition more comparable across a single run, the total number of reads per gene was normalised to the total number of sequencing reads for the "+0.5 mM" condition (which displayed the largest number of reads for both runs). 0.1 was added to prevent division by 0 when calculating the insertion indexes for Data S1B. (B) Average fold change in the number of insertions (log2) in the indicated concentration of NaN3 compared to growth in its absence.

Data S2. Transcriptional profiling of azide treated cells. A culture of *E.coli* BW25113 in exponential phase was divided. Half was treated with 2 mM NaN_3 for 10 minutes. mRNA was prepped from the treated and untreated samples and changes in mRNA levels were determined using a DNA microarray. (A) Expression profiling data of E. coli BW25113 treated with 2 mM NaN3 for 10 minutes compared to untreated cells. Listed are the Blattner accession number for each gene, the common name for the gene (from EcoCyc) and the $\log_{10}$ of the fold change in mRNA level. (B) Regulators controlling the expression of genes displaying a > $10^{0.5}$-fold or <$10^{-0.5}$-fold change in mRNA levels. Regulators were determined from RegulonDB. (C) Regulators grouped by functional category. Regulators were grouped into the categories given at http://www.mrc-lmb.cam.ac.uk/genomes/madanm/reports/tf92info.html except for metal-binding regulatory proteins, which were determined manually.

Table 1. Effect of metal availability on the sensitivity of *E. coli* MC4100 and *azi* mutants to azide.

Strain	Substitution[a]	Zone of clearing[b]			
		LB[c]	+EDTA[c]	+$FeSO_4$[c]	+$ZnSO_4$[c]
MC4100 (*secA*$^+$)	N/A	27.3 ± 2.4	33.3 ± 2.4	24.5 ± 0.5	28.5 ± 1.5
azi-1	N379I	18.3 ± 0.3	13.0 ± 1.0	ND[d]	ND[d]
azi-4	L645Q	19.3 ± 0.3	16.5 ± 0.5	ND[d]	ND[d]
azi-5	L645Q	17.0 ± 3.0	9.5 ± 0.5	ND[d]	ND[d]
azi-7	L179Y	< 6	10.5 ± 4.5	ND[d]	ND[d]
azi-8	R561H	15.0 ± 1.0	8.5 ± 2.5	ND[d]	ND[d]
azi-16	L515F	23.5 ± 5.5	14.0 ± 8.0	ND[d]	ND[d]
azi-D1	T130I	19.0 ± 2.9	12.8 ± 1.3	ND[d]	ND[d]
azi-D2	Y186D	19.7 ± 3.0	< 6	ND[d]	ND[d]

[a]Amino acid substitution encoded by azi mutation.

[b]The diameter of the zone of clearing in a confluent lawn of bacteria surrounding a 6 mm antibiotic assay disc containing 10 μl of a 1 M solution of NaN_3; units in mm. Confidence intervals are one s.d.

[c]Azide was determined on LB agar plates. Where indicated, EDTA (1 mM), $FeSO_4$ (100 μM) or $ZnSO_4$ (100 μM) was incorporated into the growth media. Confidence intervals are one s.d.

[d]Not determined

Table 2. Growth of *E. coli* MC4100 and *azi* mutants in M63 (low Fe) media.

		Doubling time first growth phase[b]				
Strain	**Substitution[a]**	**M63 (low Fe)[c]**	**+EDTA[c]**	**+EDTA +$FeCl_3$[c]**	**Cell density at onset of first diauxic shift[d]**	**Recovery[d]**
MC4100 (*secA*$^+$)	N/A	82.8 ± 1.1	118.7 ± 6.1	82.7 ± 4.0	0.53 ± 0.02	66 ± 16
azi-1	N379I	80.6 ± 10.7	127.1 ± 0.9	68.5 ± 4.2	0.59 ± 0.01	>610
azi-4	L645Q	82.2 ± 3.2	103.8 ± 8.5	73.1 ± 4.5	0.50 ± 0.07	70 ± 12
azi-5	L645Q	86.2 ± 9.0	109.9 ± 7.4	72.3 ± 7.6	0.60 ± 0.03	77 ± 6
azi-7	L179Y	94.9 ± 3.6	125.0 ± 20.5	76.7 ± 6.9	0.55 ± 0.01	197 ± 15
azi-8	R561H	85.5 ± 1.2	119.0 ± 3.6	71.9 ± 8.3	0.52 ± 0.03	>610
azi-16	L515F	86.2 ± 7.8	104.2 ± 1.8	73.3 ± 1.7	0.59 ± 0.01	60 ± 10
azi-D1	T130I	94.9 ± 4.9	112.8 ± 5.0	71.1 ± 2.3	0.60 ± 0.01	113 ± 6
azi-D2	Y186D	80.6 ± 1.9	107.1 ± 6.0	86.0 ± 9.2	0.56 ± 0.03	64 ± 19

[a]Amino acid substitution encoded by *azi* mutation

[b]In minutes. Confidence intervals are one s.d.

[c]M63 containing 0.2% glucose from which $FeSO_4$ has been omitted. Where indicated, EDTA (10 μM) or $FeCl_3$ (20 μM) were added to the growth media. Confidence intervals are one s.d.

[d]In M63(low iron), units in OD_{600}. Confidence intervals are one s.d.

[e]The amount of time between the initial decrease in the growth rate of the first exponential growth phase and the maximum growth rate in the second exponential growth phase in M63(low iron), units in minutes. Confidence intervals are one s.d.

Figure 1.

A

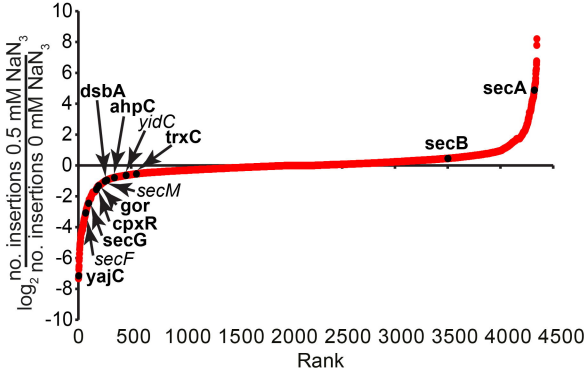
log2 no. insertions 0.5 mM NaN3 / no. insertions 0 mM NaN3
10
8
6
4
2
0
-2
-4
-6
-8
-10
0
500
1000
1500
2000
2500
3000
3500
4000
4500
Rank
dsbA
ahpC
yidC
trxC
secA
secB
secM
gor
cpxR
secG
secF
yajC

B

LB
+0.25 mM NaN3
+0.5 mM NaN3
23
0
no. insertions
secA
codon 822

C

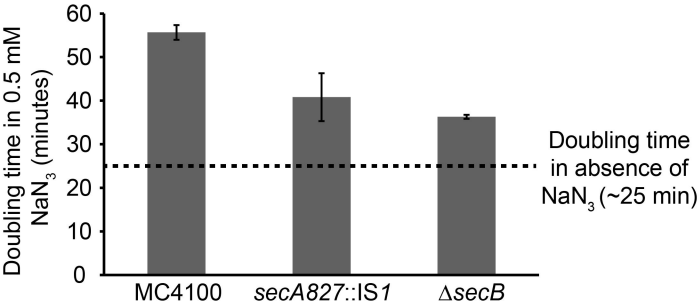
Doubling time in 0.5 mM NaN3 (minutes)
60
50
40
30
20
10
0
MC4100
secA827::IS1
ΔsecB
Doubling time in absence of NaN3 (~25 min)

Figure 2.

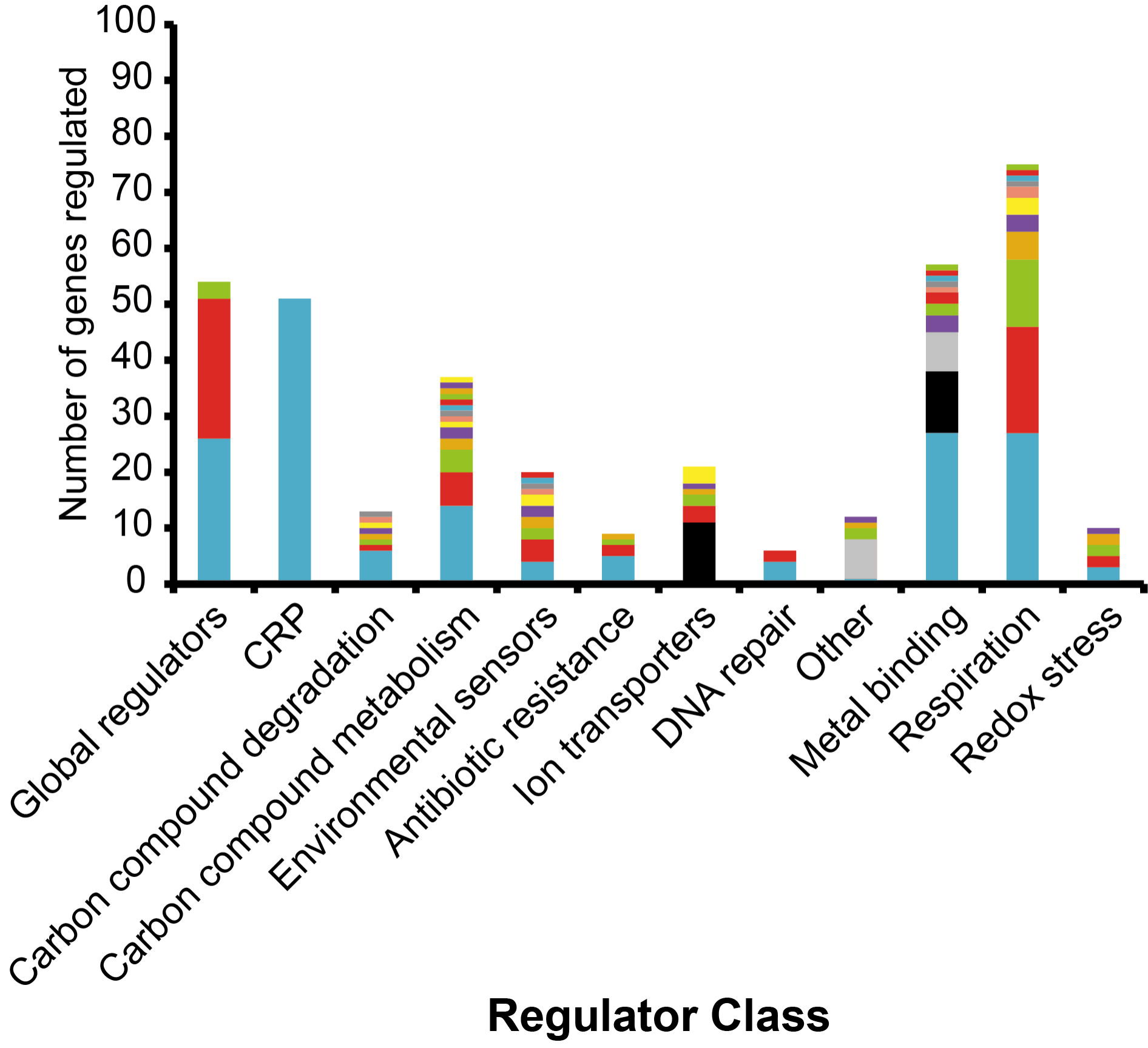
Number of genes regulated
100
90
80
70
60
50
40
30
20
10
0
Global regulators
CRP
Carbon compound degradation
Carbon compound metabolism
Environmental sensors
Antibiotic resistance
Ion transporters
DNA repair
Other
Metal binding
Respiration
Redox stress
Regulator Class

Figure 3.

A

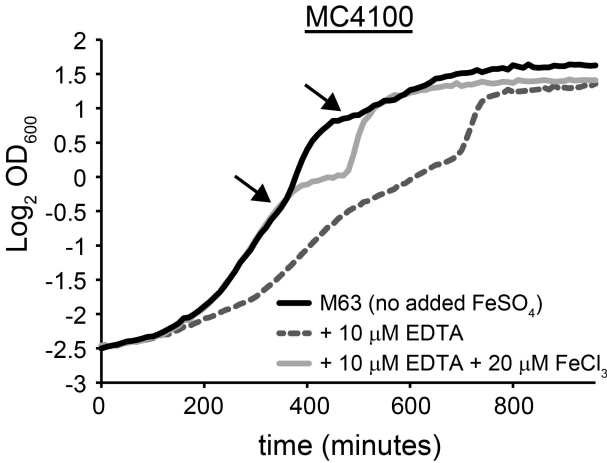
MC4100
Log2 OD600
2
1.5
1
0.5
0
-0.5
-1
-1.5
-2
-2.5
-3
0
200
400
600
800
time (minutes)
M63 (no added FeSO4)
+ 10 μM EDTA
+ 10 μM EDTA + 20 μM FeCl3

B

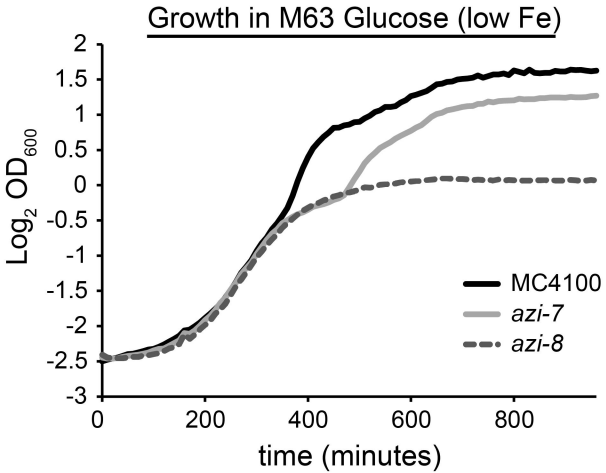
Growth in M63 Glucose (low Fe)
Log2 OD600
2
1.5
1
0.5
0
-0.5
-1
-1.5
-2
-2.5
-3
0
200
400
600
800
time (minutes)
MC4100
azi-7
azi-8

Figure 4.

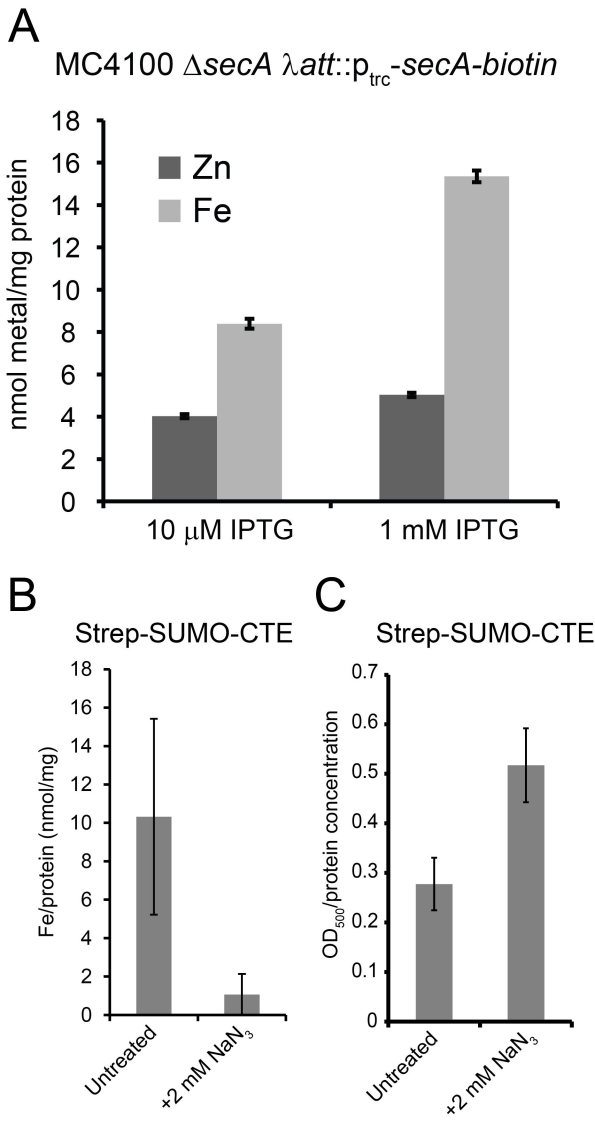
A
MC4100 ΔsecA λatt::ptrc-secA-biotin
nmol metal/mg protein
Zn
Fe
10 μM IPTG
1 mM IPTG
B
Strep-SUMO-CTE
Fe/protein (nmol/mg)
Untreated
+2 mM NaN3
C
Strep-SUMO-CTE
OD500/protein concentration
Untreated
+2 mM NaN3

Figure 5.

A

```
E. coli (MeBDwt)    GERKVGRNDPCPCGSGKKYKQCHGRLQ-- 901
R. loti             TWGKVGRNEACPCGSGKKYKHCHGAFA-- 910
B. subtilis         KVVDIGRNAPCHCGSGKKYKNCCGRTE-- 841
L. lactis           SFENVGRNDLCPCGSGKKFKNCHGRTHIA 865
T. pallidum         AGAKVGRNTPCPCGSGKKYKHCCGR---- 916
B. longum           TFPGTGKNAPCPCGSGRKYKMCHGQNEA- 964
B. thetaiotamicron  AEKTVGRNDPCPCGSGKKYKNCHGQNA-- 1106
MeBD-S15A           GERKVGRNDPCPCGAGKKYKQCHGRLQ--
                         *:*  * ****:*:* * *
```

B

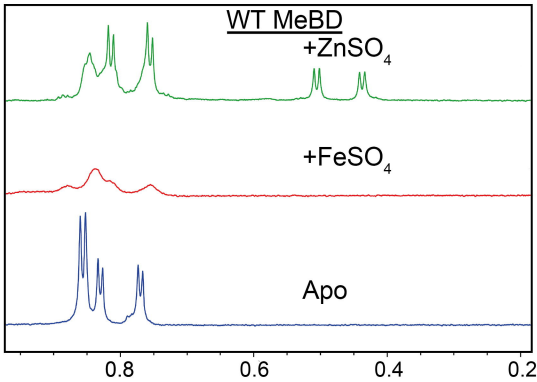

C

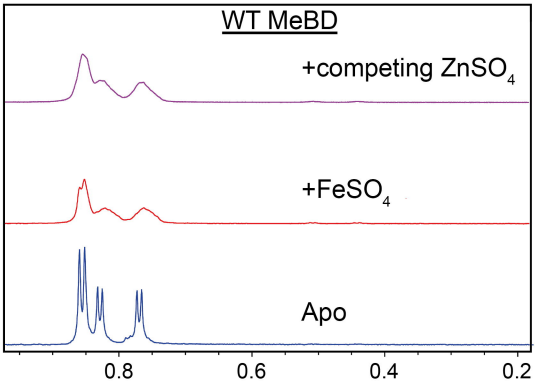

D

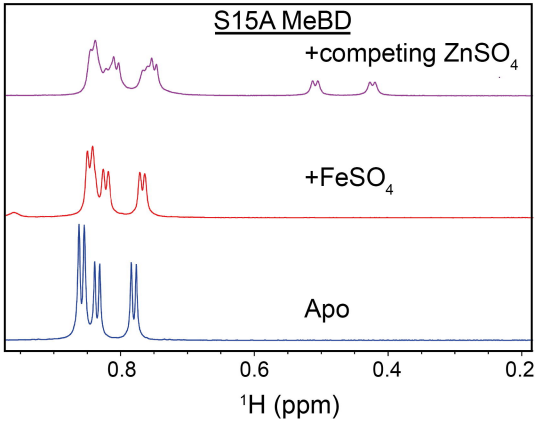

Figure 6.

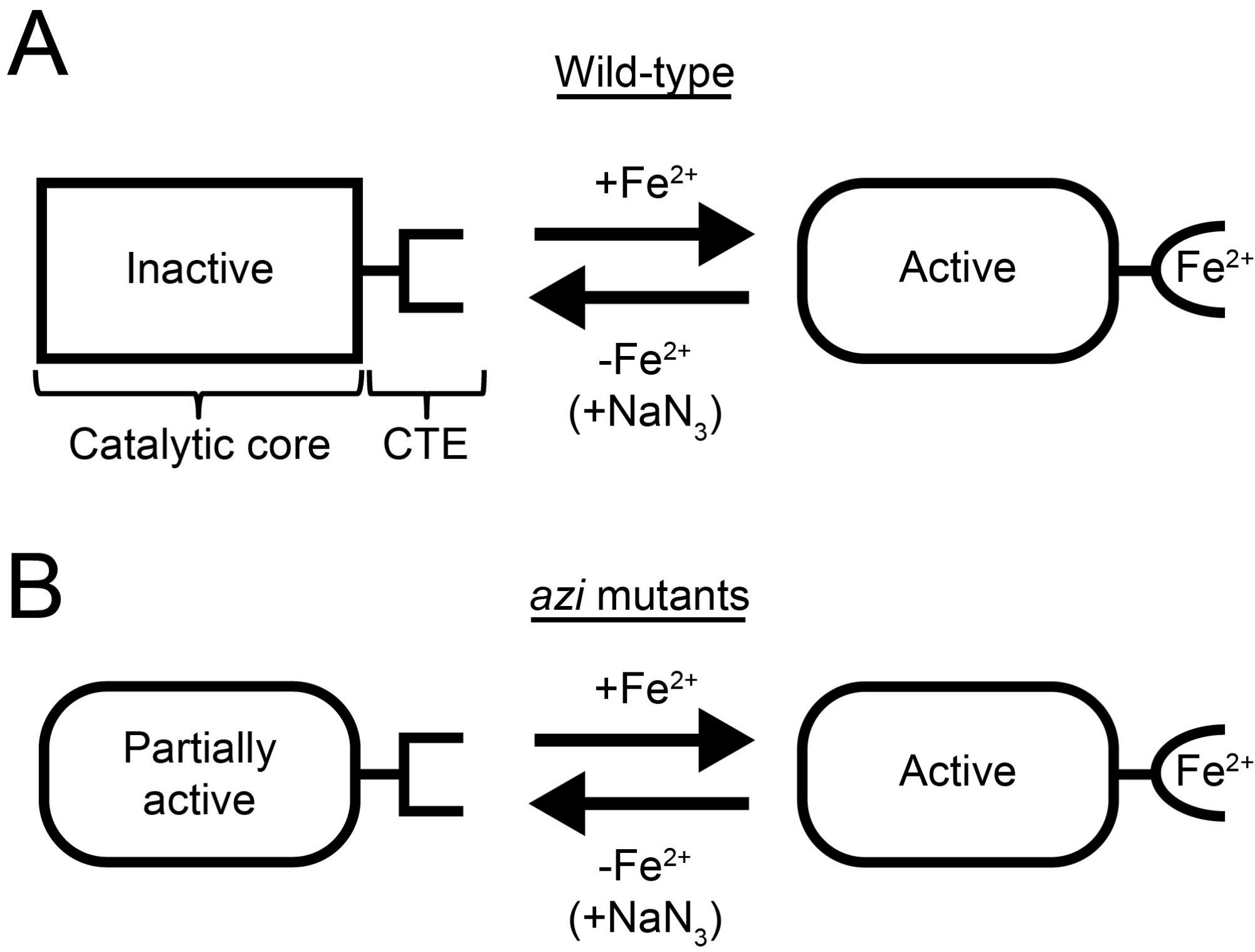
A
Wild-type
Inactive
+Fe2+
-Fe2+
(+NaN3)
Active
Fe2+
Catalytic core
CTE
B
azi mutants
Partially active
+Fe2+
-Fe2+
(+NaN3)
Active
Fe2+